Fermi Surface of Mg_2Pb†

G. A. Stringer* and R. J. Higgins
University of Oregon, Eugene, Oregon 97403
(Received 10 March 1970)

Experimental observations are reported of Landau quantum oscillations (LQO) in the electrical transport properties of the compound Mg_2Pb in the range $H \leq 50$ kG and $T = 1.2$–4.2 °K. The results are associated with two bands of holes previously inferred in explaining the low-field ($H \leq 5$ kG) field dependence of the Hall coefficient, confirming the earlier interpretation. The magnetoconductivity tensor elements derived from the *nonoscillatory* contributions to the Hall and transverse magnetoresistivity have been fitted with three bands of carriers labeled as light holes, heavy holes, and electrons. This establishes band overlap in Mg_2Pb. The light-hole band ($F = 0.27 \times 10^6$ G) is nearly spherical (±2%) with $m^* \simeq 0.04 m_e$, $g \simeq 11$, and contains 7.9×10^{17} carriers/cm^3. The heavy-hole band [$F = (2.8$–$3.7) \times 10^6$ G] is a warped sphere, whose shape has been determined from experimental extremal cross sections using the Fermi-radius inversion method developed by Mueller. The heavy-hole cyclotron effective mass has been measured as 0.35 and 0.45 electron masses for orbits perpendicular to [100] and [111], respectively. This band contains 4.2×10^{19} carriers/cm^3. These two valence bands are compared with similar valence bands in Ge via the model of Dresselhaus *et al.* The evidence for a Ge-like, rather than grey-Sn-like, valence-band ordering is consistent with the band calculation of Van Dyke and Herman. No LQO associated with the electron band were observed, although the analysis of classical magnetoconductivity data requires the presence of 4.1×10^{19} electrons/cm^3 in order to explain the high-field value of $H\sigma_{12}$.

I. INTRODUCTION

In spite of the high proportion of good metals in the system of intermetallic compounds Mg_2X (X is Si, Ge, Sn, or Pb), all of the members are relatively poor electrical conductors,[1–4] the first three members being semiconductors, while Mg_2Pb is semimetallic. This behavior was first interpreted by Mott and Jones on the basis of the electronic band structure.[5] They noted that the number of valence electrons was just enough to fill the first four Brillouin zones of the fcc Bravais lattice (anti-CaF_2 crystal structure). Later, measurements of the electrical properties of this system were aimed primarily at discovering and developing possible technological applications.[6–9] In addition, there was interest in both experimental and theoretical determinations of the band structure. Most of the experimental efforts in band-structure determination were directed toward Mg_2Sn,[10–12] while theoretical work until recently had generally been on the lighter members of the group.[13–17] Although the experimental studies revealed many of the qualitative features of the band structure, few if any measurements offered a direct quantitative comparison between theory and experiment. The purpose of this paper is to report on such a series of measurements which have been made on the least understood compound in this system: Mg_2Pb.

Until recently, only sketchy and somewhat contradictory information on the electrical properties of this compound was available.[2,3,18] Recently, we reported the low-field ($H < 5$ kG) galvanomagnetic properties of Mg_2Pb.[19] On the basis of those observations it appeared that quantitative measurement of some Fermi-surface (FS) parameters would be possible at high magnetic fields. We report here measurements of the magnetoresistance and Hall voltages in magnetic fields up to 50 kG and at temperatures from 1.12 to 4.2 °K which exhibit Landau quantum oscillations (LQO) in these properties, in addition to their normal monotonic variations. Extremal cross-sectional areas, effective masses, and effective scattering temperatures are deduced from these measurements for several orbits on two different sheets of the FS.

In the earlier low-field measurements,[19] it was possible to explain the field dependence of the Hall coefficient in terms of two spherical bands, the light and heavy holes. Both the Hall coefficient and magnetoresistance were consistent with this model and quite similar in behavior to p-type Ge.[20] However, extension of these measurements to 5 kG $< H <$ 40 kG reveals that the two-band model is unable to account for the observed behavior, as shown in Fig. 1. According to the two-band model, whose parameters were determined at low fields, the Hall coefficient would be expected to saturate at high magnetic fields at the value R_∞, which is clearly not the case. These observations require, in addition, a third band of carriers. The analysis is carried out using the magnetoconductivity tensor, since the contributions of every band are then additive and of the same simple form.[21] With this anal-

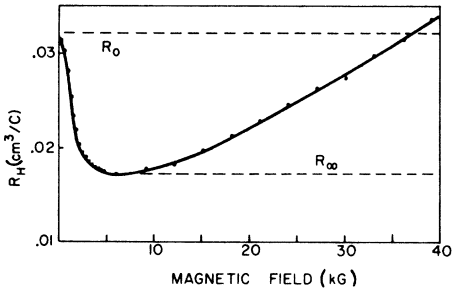

FIG. 1. Magnetic field dependence of the Hall coefficient showing the high-field departure from the low-field two-band model. R_0 and R_∞ (Ref. 19) show the low- and high-field values expected if only the two-hole bands are present.

ysis, it is possible to compare the results obtained from the LQO measurements, and, further, to show that electrical transport in Mg_2Pb involves not only two bands of holes but also electrons, establishing unambiguously the existence of band overlap.

II. EXPERIMENTAL PROCEDURE

Details of crystal growth and sample preparation are given elsewhere.[19] The residual-resistance ratio ($R_{273}/R_{4.2}$) was typically 25. Both dc and ac techniques were used to measure the magnetoresistance and Hall voltages. The dc four-probe method is illustrated by the schematic diagram shown in Fig. 2. In these measurements, the sample (No. 1b, $1.2\times1.3\times10$ mm) was held with the current fixed along $[11\bar{2}]$ and the magnetic field along one of three fixed orientations, [100], [110], or [111]. The last orientation was the transverse magnetoresistance configuration ($\vec{H}\perp\vec{J}$) and was used in measuring the total dc variations of the magnetoresistance and Hall voltages which were later inverted to the magnetoconductivity. In these measurements, the bandpass filter was eliminated and the output of the nanovoltmeter was recorded directly on the XY recorder as a function of the superconducting solenoid current. Traces of LQO superposed on the monotonic background were observed both in the dc magnetoresistance and Hall voltage, although the dominant LQO frequency differed in the two cases. The lower-frequency LQO corresponding to the minority light holes was dominant in the Hall voltage, while the higher frequencies corresponding to the majority heavy holes were most prominent in the magnetoresistance. With $1/H$ swept linearly in time, the LQO are periodic in time. The bandpass filter was used to isolate different oscillatory frequencies in the spectrum and study the field dependence of their amplitude for use in calculating effective masses and scattering temperatures. Although the Kronhite filter proved exceedingly useful in separating the small LQO from a larger monotonic background, it introduced a frequency-dependent phase shift between the input and the output signals. This effect produced no error in the measurement of the oscillatory frequency (since the LQO were periodic in time) but, to avoid errors in effective mass determination, it was necessary to average between an upsweep and a downsweep in order to associate an *amplitude* with a particular value of magnetic field strength.

Because of the frequency-dependent phase shift, LQO waveforms containing high-harmonic content were distorted when passed through the filter. Since the low-frequency LQO exhibited structure interpreted as spin splitting, and since an accurate record of the undistorted waveform is required for determination of the g factor, another method was used to reduce the large nonoscillatory background signal. An admixture of the monotonic magnetoresistance signal, introduced into the Hall voltage by misalignment of the pressure contacts, was used to nearly cancel the monotonic Hall voltage. By properly choosing the direction of the magnetic field, the contributions from the Hall effect (odd in H), could be made to nearly cancel the contributions of the magnetoresistance error signal (even in H) over a portion of the field sweep. In this way, it was possible to measure the spin splitting from LQO waveforms recorded without filtering.

Investigations of the angular dependence of the LQO frequency spectrum were made using a spiral-geared sample holder which allowed continuous angular rotation with respect to the direction of the magnetic field. A diagram of the experimental apparatus is shown in Fig. 3. The chief source of angular error in this apparatus was backlash, the

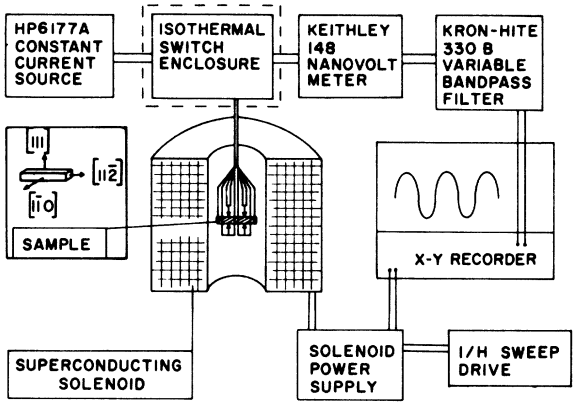

FIG. 2. Schematic diagram of apparatus used to make dc measurements. The bandpass filter was used only when studying LQO to eliminate monotonic variations and select single-oscillatory frequencies. The sample holder allowed selection of several fixed orientations with respect to $\vec{H}$.

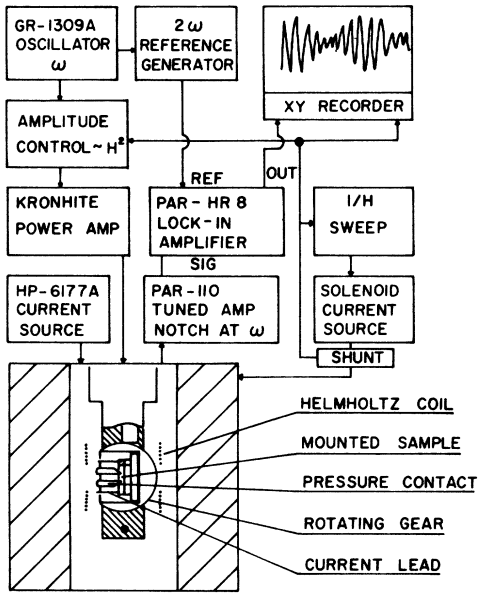

FIG. 3. Schematic diagram of field-modulation apparatus used to study angular dependence of LQO spectrum. The second harmonic of the 15-Hz modulation signal was synchronously detected and plotted inverse magnetic field on an XY recorder. The sample orientation was varied by means of a spiral-toothed gear whose axis of rotation was perpendicular to $\vec{H}$. The sample was contained in a cylindrical hole in the gear and could be rotated to preselect any plane of rotation.

effects of which could be eliminated by reaching any orientation through a final rotation always in one direction.[22] The final orientation of the sample holder with respect to the rotating gear (which determined the plane of rotation) was accomplished using an optical lever arrangement.[23] In these experiments, the field-modulation technique (FMT)[24] was used with phase-sensitive detection of the ac component of the magnetoresistance voltage. The second harmonic of the 15 Hz modulation was detected and recorded as a function of $1/H$ on an XY recorder. The modulation amplitude was adjusted to maximize the LQO and maintained at an optimum level by varying the modulation amplitude proportional to H^2, using a Servo system.[25]

III. MAGNETIC FIELD DEPENDENCE OF ELECTRICAL CONDUCTIVITY TENSOR

A. Theory of Classical Multiple-Band Magnetoconductivity

The isothermal conductivity tensor $\overleftrightarrow{\sigma}$ is defined by the equation

$$\vec{J} = \overleftrightarrow{\sigma} \cdot \vec{E} , \tag{1}$$

where $\vec{J}$ is the current density and $\vec{E}$ is the electric field. The z axis is defined by the magnetic field $\vec{H}$ which, for experimental reasons,[26] was chosen to lie along the [111] axis of this cubic crystal. In the relaxation-time approximation, the magnetic-field-dependent elements of the conductivity tensor have the following approximate form:

$$\sigma_{11} = \sigma_{22} = \sum_i n_i e H_i [H^2 + H_i^2]^{-1} , \tag{2a}$$

$$\sigma_{12} = -\sigma_{21} = \sum_i n_i e H [H^2 + H_i^2]^{-1} , \tag{2b}$$

where n_i and H_i are model parameters, which, in the special case of spherical bands, are the number of carriers and inverse Hall mobility ($H_i = n_i e/\sigma_i$) for the ith band. The summation is carried out over all bands of carriers.

Equation (2a) is a sum of Lorentzian functions of H each of which contains a weighting factor proportional to the partial conductivity σ_i for the ith band. It will be convenient to rearrange (2b) in two different forms in order to emphasize two different physical properties and the distinct characteristics of the low-field and high-field regimes. Both of these forms retain the Lorentzian line shape. The first rearrangement of (2b),

$$\sigma_{12}/H = \sum_i (n_i e/H_i^2)[1 + (H/H_i)^2]^{-1}, \tag{3}$$

yields a sum of Lorentzian functions of H containing weighting factors proportional to the carrier mobility in the ith band. This representation of the data emphasizes the details of the low-field behavior of σ_{12}. The high-field behavior is more easily seen in the other useful form of (2b),

$$\sigma_{12} H = \sum_i n_i e[1 + (H_i/H)^2]^{-1} , \tag{4}$$

which is a sum of Lorentzian functions of $1/H$ with weighting factors proportional to the number of carriers in the ith band. This analysis gives a good fit to the data in spite of the obvious deficiencies of the simple model[27] and provides independent qualitative information about the band structure of Mg_2Pb in support of, and in addition to, that obtainable from the LQO data.

B. Magnetoconductivity Observations and Band-Model Deductions

The experimental values of σ_{11}, σ_{12}/H, and $\sigma_{12}H$ were calculated from the measured resistivity tensor using the inversion relations

$$\sigma_{11} = (\rho_{11})^{-1}[1 + (RH/\rho_{11})^2]^{-1} , \tag{5a}$$

$$\sigma_{12} = \sigma_{11}(RH/\rho_{11}) , \tag{5b}$$

where ρ_{11} is the measured transverse magnetoresistivity and RH is the measured Hall resistivity. All other independent elements of the conductivity tensor are zero by symmetry in this orientation.

The results, shown in Figs. 4–6 require a three-band version of the model described above in order to reproduce all of the qualitative features. The dashed curves are the contributions to the total conductivity of each band as determined by a least-squares fit to the model expressed in Eqs. (2a),

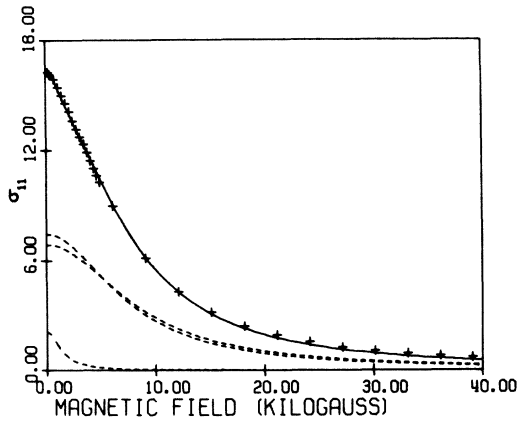

FIG. 4. $\sigma_{11}(10^4/\Omega\,\mathrm{cm})$ versus H (kG). The data (+) are determined from the magnetoresistance and Hall voltages using Eqs. (5a) and (5b). The solid curve is the least-squares fit to the data by a function having the form of Eq. (2a) and the dashed Lorentzians show the contributions from each of the three bands assumed in the model.

(3), and (4).[21] The fitting procedure selected two parameters n_i and H_i for each band subject to the condition that the total rms deviation of the fitted curve from the data be minimized. The values of the six parameters determined by the fitting procedure are shown in Table I, along with mobilities derived from the classical interpretation of H_i.[28] The bands 1–3 have been identified with light holes, heavy holes, and electrons, respectively. The observation of LQO (Sec. IV) confirms the existence

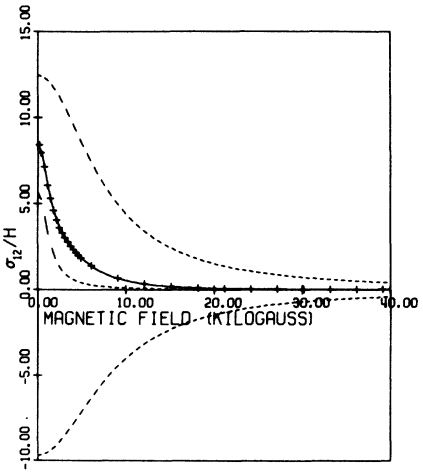

FIG. 5. $\sigma_{12}\,(\mathrm{G}\,\Omega\,\mathrm{cm})^{-1}$ versus H (kG) emphasizes low-field properties. The data points have been fit to an expression of the form shown in Eq. (3). The contributions of the individual bands are shown as dashed curves. Positive curves correspond to holes while the negative curve represents electrons.

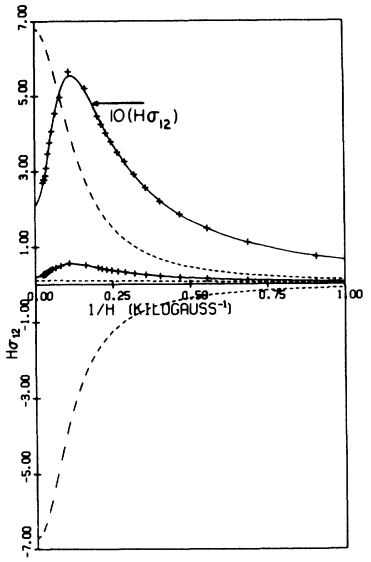

FIG. 6. $H\sigma_{12}$ (10^8 G/Ω cm) versus $1/H$ (kG^{-1}) emphasizes high-field properties. This representation of the data clearly shows that electrical transport in Mg_2Pb involves both holes and electrons, i.e., it is impossible to fit the data with an expression having the form of Eq. (4) without having both positive and negative Lorentzians. Again, the dashed curves show the contributions of the individual bands. Since the heavy-hole and electron-band contributions are each much larger than the experimental data, a ten times expanded view of the data and three-band fit are also shown (upper solid curve).

of the first two, but not the third band of carriers. It is important to note, however, that the only way to fit the peaked curve of Fig. 6 is with a superposition of positive (holes) and negative (electrons) Lorentzians. This information, together with the knowledge that the carriers are degenerate, leads to the unambiguous conclusion that band overlap occurs in Mg_2Pb.

IV. LANDAU QUANTUM-OSCILLATION MEASUREMENTS

A. Theory of Quantum Oscillations in Magnetoresistance

LQO in the magnetoresistance, commonly called the Shubnikov–de Haas effect,[29] are produced by a modulation in the density of states at the FS in the presence of a changing magnetic field. The theory is treated elsewhere.[30] Such oscillatory phenomena arise from the quantization of electron energy levels (Landau levels) whose energy spacings are proportional to the applied magnetic field, resulting in LQO which are periodic in inverse field. The frequency F gives a means of directly measuring the extremal cross-sectional area A of the FS in the direction defined by $\vec{H}$, through the relation

$$F = c\hbar A/2\pi e\ . \qquad (6)$$

TABLE I. Summary of band parameters (n_i, H_i) obtained from a least-squares fit to the magnetic field dependence of the magnetoconductivity tensor. The values for σ_i and μ_i were calculated from the parameters using the classical relationships indicated.

Band label	1	2	3
H_i (kG)	1.2	7.1	− 8.2
$\mu_i = 10^8/H_i$ (cm^2/V sec)	8.3×10^4	1.4×10^4	-1.2×10^4
n_i (cm^{-3})	5.4×10^{17} holes	3.6×10^{19} holes	3.5×10^{19} electrons
$\sigma_i = n_i e\mu_i$ $(\Omega\,\mathrm{cm})^{-1}$	7×10^3	8.1×10^4	6.9×10^4

The amplitude of the oscillatory magnetoresistance

$$\frac{\Delta\rho_{LQO}}{\rho(H)} \propto \frac{(T+T_I)e^{-\beta^* T_D/H}}{H^{1/2}\sinh[\beta^*(T+T_I)/H]} \tag{7}$$

[where $\beta^* = 2\pi^2 km^* c/e\hbar = 1.468(m^*/m_e)\times10^5$ G/°K], can be used to extract experimental values for the effective mass m^*, the effective scattering temperature T_D, and the effective temperature due to inhomogeneity broadening T_I, from the temperature and field dependence of the LQO amplitude.[31]

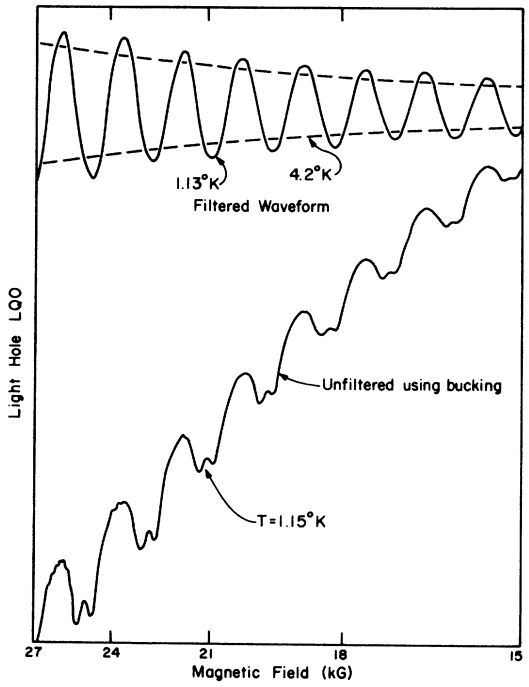

FIG. 7. Typical LQO observed from the light-hole carriers. The lower curve shows an unfiltered dc waveform obtained using the approximate bucking scheme described in the text. Spin splitting of the peaks is evident. The upper curve was filtered and shows the effect of removing the harmonic content from the lower waveform. The dashed lines show the change in amplitude as T was increased from 1.13 to 4.2°K.

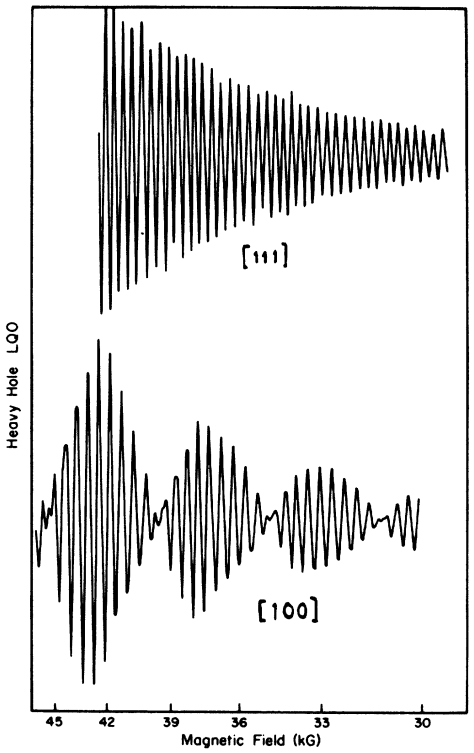

FIG. 8. Typical LQO observed from the heavy holes using filtering. Frequencies and effective masses were nearly the same for $\vec{H}$ in [111] and [110]. Two lower frequencies were observed with $\vec{H}$ in [100].

B. Experimental LQO Spectra

Typical records of the LQO observed in sample 1b using the dc method are shown in Figs. 7 and 8. In all of the records, the bandpass filter was used to eliminate the monotonic background signal, except for the lower trace in Fig. 7 (light holes) which illustrates the approximate bucking method. The spin splitting which is apparent in this unfiltered waveform is completely eliminated in the filtered version shown above it. The change in amplitude of the fundamental frequency with temperature (dashed lines show the envelope at 4.2 °K) was used to estimate the effective mass for these carriers. These results are shown in Table II along with other numerical results from the LQO analysis. The fact that the change in amplitude was comparable to the noise is reflected in a large uncertainty for m^* and also for g. Typical LQO for the heavy holes are shown in Fig. 8. Filtering has been used to suppress the light-hole LQO. Table II shows the cyclotron effective masses measured at three symmetry directions. Within experimental error, the

TABLE II. Band parameters obtained from quantum-oscillation measurements. The g factor was obtained by associating the split minima in Fig. 7 with spin-split Landau levels, with a phase shift 2π ($gm^*/2m_e$).

	Light holes	Heavy holes
LQO frequency F	0.27×10^6 G	$2.7-3.8\times10^6$ G
FS shape	Spherical	Warped sphere
Effective mass m^*/m_e	0.04 ± 0.01	0.35 ± 0.02 in [100] 0.45 ± 0.06 in [111], [110]
Scattering temperature T_D	•••	(1.2 ± 0.3) °K
g factor	11 ± 2.5	•••
number of carriers n	7.9×10^{17} cm^{-3}	4.2×10^{19} cm^{-3}

same mass was estimated for both [110] and [1$\bar{1}$1] orientations. When $\vec{H}$ was along [1$\bar{1}$1] ($\vec{H}\perp\vec{J}$), it was possible to estimate the effective scattering temperature T_D from the field dependence of $\Delta\rho_{LQO}/\rho(H)$.

The LQO observed with $\vec{H}$ in [100] exhibit strong beating effects from two oscillations of nearly equal amplitude. The effective mass determined from these two competing frequencies represents an average over two different orbits. At low fields the lower frequency was dominant, while at higher fields the upper frequency became dominant indicating a slightly higher effective mass for the larger orbit. In addition, at high fields a signal was observed arising from harmonics of the two fundamental LQO. Analysis of the actual wave shape clearly shows that the higher frequency arises from a relative maximum in the cross-sectional area, while the other is due to a minimum.[32] This observation is compatible with the orbital assignments discussed below. LQO frequencies observed for the heavy holes in two principal symmetry planes are shown in Fig. 9.

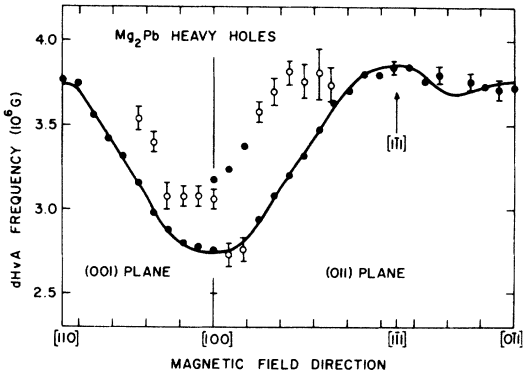

FIG. 9. Angular dependence of the LQO frequency spectrum for the heavy-hole band with $\vec{H}$ in the (001) and (011) planes. The solid curve represents the least-squares fit. Solid circles designate the LQO frequency of dominant amplitude, while open circles are frequencies deduced from beats.

TABLE III. Geometry of the heavy-hole band. Experimental areas A are measured in wave-number units $(2\pi/\text{Å})^2$ and directions designate normals to the plane of the orbit. Fermi radii along the directions specified are derived from the Mueller inversion scheme and have units of $(2\pi/\text{Å})$.

	[100]	[110]	[111]
A	0.0264	0.0360	0.0367
k_F	0.0692	0.1093	0.1262

C. Experimental Fermi-Surface Deductions

Two sheets of the FS of Mg_2Pb have been resolved in these measurements; the light and heavy holes. The labeling as holes comes partially from the symmetry of the LQO observations and by correspondence with the highest-mobility-carrier species determined in Sec. III; the evidence for this identification will be discussed in Sec. V. While the light holes have identical extremal areas at the three symmetry directions measured, the heavy-hole cross sections have a large anisotropy ($A[111] \gtrsim A[110] > A[100]$) as shown in Table III. The observed angular dependence of areas (Fig. 9) are consistent with central cross sections of a closed single centrosymmetric surface (therefore centered at Γ in the Brillouin zone). The surface also supports a noncentral extremal area for field directions near [100], which is larger in cross section than the central extremum. These observations require the surface to be a warped sphere, with Fermi radii such that $k_F[111] \gtrsim k_F[110] > k_F[100]$.

Although observed extremal areas can be compared with areas calculated from a given model, such calculations are tedious for a highly warped sphere, and the resulting parameters are not necessarily unique and highly model dependent. Instead, one can calculate Fermi radii directly from experiment, using a theorem due to Lifshitz and Pogorelov[33] which was first brought to practical utility by Mueller and Priestly.[34] The set of observed central extremal cross section are fit by a linear combination of cubic harmonics

$$A(\theta,\phi)=\sum_{l,t} {}_t\beta_l\ {}_tK_l(\theta,\phi)\ , \tag{8}$$

with the expansion coefficients ${}_t\beta_l$ determined from a least-squares fit to data in the (001) and (011) planes. Under these conditions, 11 expansion coefficients can be determined uniquely. But the Mueller inversion theorem[35] shows that the Fermi radii are determined by a similar expansion, with expansion coefficients related in a simple way to the area

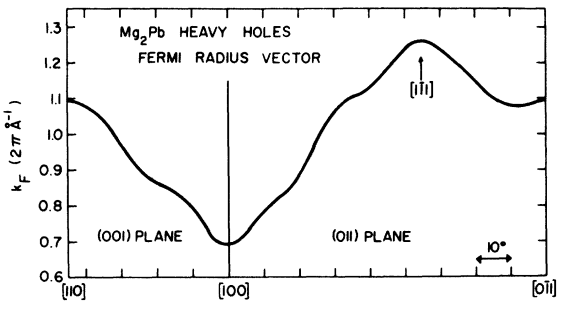

FIG. 10. Fermi-radius vector for the heavy holes of Mg_2Pb, determined by fitting the observed extremal areas (Fig. 9) using the Mueller inversion scheme.

expansion coefficients

$$k_F^2(\theta,\phi)=\sum_{l,l}\frac{{}_l\beta_l}{\pi P_l(0)}\,{}_lK_l(\theta,\phi)\,. \tag{9}$$

This procedure was carried out for the heavy holes in Mg_2Pb. But the inversion theorem applies only to the central extremal area, and the data shows two extrema near [100]. The lower-branch data were used in the fit, for reasons discussed below. The least-squares fit (Fig. 9, solid curve) was in excellent agreement with the data. The resulting Fermi-radius vector (Fig. 10) has the expected qualitative behavior, as shown in Table III. The surface is nearly cubic in shape, as is shown clearly in a polar plot (Fig. 11). The "cube" is rounded at the edges and corners, and pushed in along [100] directions.

These results, though model independent, are subject to certain errors due to experimental uncertainties in the measured cross sections, and due to the small set of expansion coefficients used. Although the gross features of Figs. 10 and 11 are not likely to change, we do not feel confident at present about the fine ripples. For example, in the metal Pd, which has a rapid variation in area near [110], early results[36] showed a small extra bump in Fermi radius which vanished in more refined analysis of more precise data.[37] Viewing the method as a Fourier analysis, any rapid change requires high-order harmonics. But in Mg_2Pb, the area variation (Fig. 9) is slower than in Pd, and the errors are of a random nature unlikely to lead to spurious higher harmonics of large amplitude.

A second extremal area (Fig. 9, upper branch) was observed near [100] and appears to merge with the dominant curve (Fig. 9) with $\vec{H}$ about 20° from [100] in the (001) plane and about 38° from [100] in the (011) plane. Although the details of this branch (particularly the merging with the dominant branch) are not fully determined, the presence of a second extremum when $\vec{H}$ is near [100] is required by the FS parameters determined from the central extremum (Fig. 9, lower branch) alone. The surface shown in Figs. 10 and 11 predicts, perpendicular to [100], in addition to the central (minimum) cross section A_0, a noncentral (maximum) cross section A whose calculated area is $(13\pm2)\%$ larger than A_0. For comparison, the second extremum observed at [100] has an area 12% larger than the dominant branch. For this reason, the second extremal area is assigned to a noncentral orbit rather than to a separate sheet of the FS. The good agreement between experimental and calculated areas supports the selection of the lower branch in Fig. 9 as the central extremum.

The resulting picture of the FS sections observed in these experiments is a nearly spherical surface nested within a larger distorted sphere (Fig. 11), both located at Γ in the Brillouin zone. This experimental conclusion bears a remarkable resemblance to the constant-energy surfaces of p-type germanium.

V. BAND MODEL FOR Mg_2Pb

Van Dyke has performed a relativistic orthogonalized-plane-wave (OPW) band-structure calculation for Mg_2Pb.[38] In this section, a qualitative comparison will be made between the experimental band-structure information reported here and the results of Van Dyke's calculation. Quantitative comparisons will be found elsewhere.[38]

The qualitative structure of the Mg_2Pb energy bands near the Fermi energy is shown in Fig. 12. The band calculation[38] gave the bands ordered as shown in Fig. 12(a), but with the Γ_6^+ conduction band in close proximity (0.15 eV) to the valence-band edge. We will show that the experimental FS data, however, are more consistent with the valence-band structure at Γ as found by Van Dyke[38] [Fig. 12(a)] than the alternative picture [Fig. 12(b)]. Calculated conduction bands are at X and L, with the level at X being the lower (in fact, showing 0.01-eV overlap with the valence band).[38] The experimental FS data are consistent with semimetallic band overlap, but are not able at present to choose between conduction bands at X or at L.

Although both experimental and calculated valence

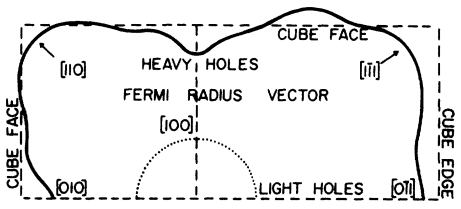

FIG. 11. Polar plot of the heavy-hole Fermi radii of Fig. 10. The straight lines define a reference cube whose faces have been chosen to coincide with the nearly flat regions in the (100) plane of the actual surface.

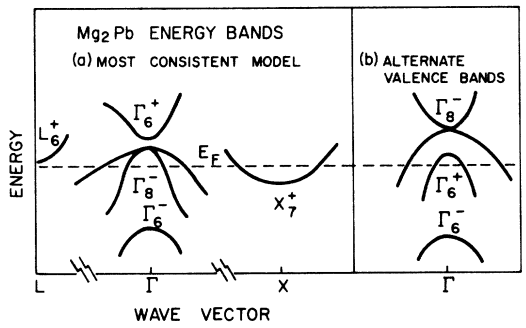

FIG. 12. (a) Qualitative features of the Mg_2Pb energy bands (Ref. 37). (b) Alternative band structure for Mg_2Pb.

bands resemble p-type germanium, there is a difference in symmetry, since in Mg_2Pb the center of symmetry is located at an atomic site. The valence-band edge in Mg_2Pb is $\Gamma_8^-(\Gamma_{15}$ without spin orbit) rather than $\Gamma_8^+(\Gamma_{25})$ as in germanium.[38] In the following discussion, the terms Ge-like [Fig. 12(a)] and Sn-like [Fig. 12(b)] are used for convenience, recognizing that a difference in symmetry exists. Although the Fermi radii of Sec. IV are of most use in quantitative comparisons with band-structure calculations,[38,39] it will be convenient here to use the Dresselhaus, Kip, and Kittel (DKK) model[40] as an aid to qualitative conclusions about the energy bands. It can be shown[39] that symmetry differences do not alter the form of the DKK second-order $E(k)$ result [Ref. 40, Eq. (63)].

A. Valence Bands

The cyclotron effective mass m^* for valence bands of the DKK form is given by [Ref. 40, Eq. (77)]

$$m^* = \frac{\hbar^2}{2(a \pm \beta)} \left(1 \pm \frac{c^2(1 - 3\cos^2\theta)^2}{64\beta(a \pm \beta)} \right) ,$$
$$\beta = [b^2 + (\tfrac{1}{2}c)^2]^{1/2} . \qquad (10)$$

Here, θ is the angle between the normal to the orbit and [100] measured in the (110) plane, and a, b, and c are the band parameters of the DKK energy spectrum

$$E(k) = ak^2 \pm [b^2k^4 + c^2(k_x^2 k_y^2 + k_y^2 k_z^2 + k_z^2 k_x^2)]^{1/2} , \quad (11)$$

when Eqs. 10 and 11 refer to holes $a < 0$, and the + and − refer to heavy and light holes, respectively. The central cross-sectional area perpendicular to each field direction in the (110) plane may be obtained from (10) using

$$A = m^* E_f (2\pi/\hbar^2), \qquad (12)$$

which is valid for bands in which the energy spectrum has the form $[k^2F(\theta, \phi)]$ as in the DKK model. It is also possible to calculate the Fermi energy E_f from the measured values for A and m^* by use of (12). E_f was calculated in the three symmetry directions for the heavy-hole band as $(9.4 \pm 0.7) \times 10^{-2}$ eV and as $(7.8 \pm 2) \times 10^{-2}$ eV for the light-hole band.[41] This agreement is consistent with a Ge-like [Fig. 12(a)] valence-band structure. This result alone does not rule out Sn-like [Fig. 12(b) valence bands, but sets an upper limit of 0.04 eV to the splitting of valence bands at Γ.

1. *Light Holes*

The number of carriers n_1 estimated for this band from the classical analysis (5.4×10^{17} cm^{-3}) is 32% lower than the number determined from the LQO frequency (7.9×10^{17} cm^{-3}). Because of the spherical character of the band (within 2% from LQO data) one might expect better agreement between the classical and quantum results. However, this large difference is most likely the result of interaction in the fitting procedure between the parameters of the light-hole band and those of the heavy-hole and electron bands where the spherical model is not justified (bands anisotropic). McClure has shown[27] that the effects of warping give rise to additional terms in the sums (2a) and (2b). The neglect of these terms in the present analysis is compensated for by a shift in the remaining parameters in order to minimize the fitting error. Therefore, if one is to expect close agreement between this type of simple classical analysis and the LQO observations, all of the bands must be spherical.

2. *Anisotropy of the Heavy-Hole Band*

If the DKK model is an appropriate form to parameterize the shape of the valence bands near Γ, and if the heavy mass carrier observed in the LQO is holelike (as deduced from the magnetoconductivity), then the shape of the heavy-hole surface is consistent with valence bands ordered as in Ge rather than as in Sn.[42] This follows from Eqs. (10) and (12) because the same combination of parameters which determines the shape of the warping of the heavy-hole surface also determines whether the light carriers are holelike or electronlike.[43] With a heavy-hole surface warped outwards at [111] and inwards at [100], it follows that the light carriers are also holelike (m^* also negative). However, this particular experimental evidence in itself does not determine the band ordering uniquely, since *deviations* from the DKK model (discussed below) partially decouple the light and heavy holes. In particular, the light holes are not accurately represented by an expression having the form of Eq. (10).

An estimate of the DKK parameters for Mg_2Pb may be made using heavy-hole extremal areas for $\vec{H}$ along [100] and [111] and the light-hole extremal

TABLE IV. Band parameters determined using Eq. (10) in units of $(\hbar^2/2m)$.

	Mg_2Pb	p Ge (Ref. 40)
a	−15.3	−13.0
$\|b\|$	12.1	8.9
$\|c\|$	11.0	10.3

area. The band parameters determined using (10) are found in Table IV.

It is unlikely that these parameter values are quantitatively reliable, since a detailed calculation[38,39] shows coupling with other bands (presumably the nearby Γ_6^+ conduction band) too strong to be treated accurately to second order (as in DKK). This shows up principally in the light holes becoming nonquadratic (though still isotropic). The present measurements are not sensitive to these corrections for the light holes because of the large uncertainty in the effective-mass measurement. However, the band calculation shows that the heavy holes remain quadratic, with an angular dependence of approximately the DKK form. Some deviation from the DKK form is evident in our experimental results for the angular dependence of area. Using (10) and (12),

$$\left[\frac{A_{\langle 111\rangle}-A_{\langle 110\rangle}}{A_{\langle 111\rangle}-A_{\langle 001\rangle}}\right] = 0.25 \text{ (DKK)}$$
$$= < 0.10 \text{ (observed)}.$$

Note that the value of this ratio in the DKK model is *independent* of the value of the DKK parameters. The discrepancy is not due to approximations made by DKK in deriving Eq. (10), since higher-order corrections due to the anisotropy are of order 1% in Ge, and the anisotropy parameter c is comparable for Mg_2Pb. The discrepancy is unlikely to be due to use of Eq. (12), good only for quadratic bands since the detailed band calculation[38] shows the heavy-hole band to be quite k^2-like in any given direction.

The number of heavy holes determined from the classical analysis (3.6×10^{19} cm^{-3}) is lower than the number estimated from an average LQO frequency (4.2×10^{19} cm^{-3}) for the band. Although the agreement is quite good, considering the departure of the band from the classical model, the number derived from the LQO frequency is probably more accurate.

B. Electron Band

The magnetoconductivity analysis shows Mg_2Pb to be a nearly compensated semimetal. The departure from perfect compensation (caused by the necessity of growing the compound from a nonstoichiometric melt)[19] is measured by the limiting behavior of $H\sigma_{12}$ as $1/H$ approaches zero (see Fig. 6).[44] This number ($p-n=1.3\times10^{18}$ cm^{-3}), along with the net hole concentration already noted above, requires a net carrier density in the electron band of 4.1×10^{19} cm^{-3}. No unambiguous LQO evidence was observed for electrons. The upper branch of the LQO spectrum (Fig. 9) is consistent with the noncentral extremal area for the heavy holes deduced from the Mueller inversion. However, the details of the beat structure are not well resolved away from [100] and may contain weak contributions from the electrons. The failure to observe LQO from the electron band, although the classical analysis (Sec. III) shows them to be only slightly less mobile than the heavy holes, may be connected with an accidental zero (or near zero) in the LQO amplitude.[32,45]

ACKNOWLEDGMENTS

The authors wish to thank J. W. McClure for many helpful discussions and suggestions on magnetoconductivity analysis, H. J. Mackey for supplying a portion of the magnetoconductivity least-squares program, J. P. Van Dyke for communicating the results of his band calculation prior to publication and advice on band-model deductions, F. M. Mueller for advice, and J. B. Ketterson for generous assistance in carrying out the Fermi-radius inversion using the computing facilities of the Argonne National Laboratory. One of the authors (G. A. S.) is indebted to R. Bowers and B. W. Maxfield for support under AEC Grant No. AT(30-1)-2150 during the time in which this paper was written.

†Research supported by the National Science Foundation and by the Tektronix Foundation.

*Present address: Laboratory of Atomic and Solid State Physics, Cornell University, Ithaca, N. Y. 14850.

[1]A. L. Norbury, Proc. Faraday Soc. 16, 570 (1921).

[2]G. Busch and U. Winkler, Helv. Phys. Acta 26, 579 (1953); Physica 20, 1067 (1954); U. Winkler, Helv. Phys. Acta 28, 635 (1955).

[3]W. D. Robertson and H. H. Uhlig, Trans. Met. Soc. AIME 96, 27 (1949).

[4]J. M. Whelan, in *Semiconductors*, edited by N. B. Hannay (Rheinhold, New York, 1960), p. 389.

[5]N. F. Mott and H. Jones, *The Theory of the Properties of Metals and Alloys* (Clarendon, Oxford, England, 1936).

[6]H. Kroemer, G. F. Day, R. D. Fairman, and J. Kinoshita, J. Appl. Phys. 36, 2461 (1965).

[7]H. P. R. Frederikse and R. F. Blunt, Proc. Inst. Radio Engrs. 43, 1828 (1955).

[8]R. Vought, U. S. Govt. Res. Rept. 39, 140 (1964).

[9]A. Stella and D. W. Lynch, J. Phys. Chem. Solids 25, 1953 (1964).

[10]B. D. Lichter, J. Electrochem. Soc. 109, 819 (1962).

[11]J. Umeda, J. Phys. Soc. Japan 19, 2052 (1964).

[12]L. D. Crossman and G. C. Danielson, Phys. Rev. 171, 867 (1968).

[13]P. M. Lee, Phys. Rev. 135, A1110 (1964).

[14]Nathan O. Folland, Phys. Rev. 158, 764 (1967); Nathan O. Folland and F. Bassani, J. Phys. Chem. Solids 29, 281 (1968).

[15]J. Della Riccia, *Proceedings International Conference on Semiconductor Physics, Prague*, 1960 (Publishing House of the Czechoslovak Academy of Sciences, Prague, 1961), p. 51.

[16]M. Y. Au-Yang and Marvin L. Cohen, Phys. Rev. 178, 1358 (1969).

[17]F. Herman, R. L. Kortum, I. B. Ortenburger, and J. P. Van Dyke, Proceedings of the International Conference on the Physics of Semiconductors, Moscow, July 1968 (unpublished).

[18]G. Busch and M. Moldovanova, Helv. Phys. Acta 35, 500 (1962).

[19]G. A. Stringer and R. J. Higgins, J. Appl. Phys. 41, 489 (1970).

[20]For a detailed review, see Albert C. Beer, *Galvanomagnetic Effects in Semiconductors* (Academic, New York, 1963), p. 175.

[21]See, for example, J. R. Sybert, H. J. Mackey, and K. L. Hathcox, Phys. Rev. 166, 710 (1968).

[22]The misorientation of the sample (No. 2b, $1.2\times1.2\times8$ mm) for measurements in the (011) plane was larger than the normal error ($\lesssim 1°$). The direction nominally referred to later as $[0\bar{1}1]$ was 3° away from $[0\bar{1}1]$ and lies in the (111) plane.

[23]See, for example, L. R. Windmiller and J. B. Ketterson, Rev. Sci. Instr. 39, 1672 (1968).

[24]D. Shoenberg and P. J. Stiles, Proc. Roy. Soc. (London) A281, 62 (1964).

[25]D. W. Terwilliger, Ph. D. thesis, University of Oregon, 1970 (unpublished).

[26]With samples cut in this configuration, only two nonzero off-diagonal elements remain in both the magnetoresistance ($\rho_{xy}=\rho_{yx}$) and conductivity ($\sigma_{xy}=\sigma_{yx}$) tensors. In addition, all of the Seitz magnetoresistance coefficients can be determined from measurements on a single sample cut in this configuration (see Ref. 11).

[27]J. W. McClure, Phys. Rev. 101, 1642 (1956).

[28]Efforts were made to determine an anisotropy parameter for each band in addition to the six parameters whose values are quoted in this model (see Ref. 21). The use of additional parameters caused convergence problems in the fitting procedure which were cured by inserting an additional constraint from the LQO data (the number of heavy holes). The parameters common to both models showed little change in going to the six-parameter model, the largest being in the number of light holes which went from 6.7×10^{17} to 5.4×10^{17} cm^{-3}. Since the use of more parameters failed to improve the overall fit to the data, and also eliminated the possibility for a completely independent determination of the band parameters (classical versus quantum measurements), the six-parameter model was adopted.

[29]L. Shubnikov and W. J. de Haas, University of Leiden Research Report No. 207a, 1930 (unpublished).

[30]See, for example, E. N. Adams and T. D. Holstein, J. Phys. Chem. Solids 10, 254 (1959); and D. E. Soule, J. W. McClure, and L. B. Smith, Phys. Rev. 134, A453 (1964).

[31]See, for example, Bruce L. Booth and A. W. Ewald, Phys. Rev. 168, 796 (1968).

[32]For a thorough discussion of LQO amplitude and waveform analysis see A. V. Gold, *Solid State Physics, Vol. I, Electrons in Metals* (Gordon and Breach, New York, 1968).

[33]I. M. Lifshitz and A. V. Pogorelov, Dokl. Akad. Nauk SSSR 96, 1143 (1954).

[34]F. M. Mueller and M. G. Priestly, Phys. Rev. 148, 638 (1966).

[35]F. M. Mueller, Phys. Rev. 148, 636 (1966).

[36]Joseph J. Vuillemin, Phys. Rev. 144, 396 (1966).

[37]L. R. Windmiller and J. B. Ketterson, Phys. Rev. Letters 20, 324 (1968).

[38]J. P. Van Dyke and F. Herman, Phys. Rev. B 2, 1644 (1970).

[39]J. P. Van Dyke (private communication).

[40]G. Dresselhaus, A. F. Kip, and C. Kittel, Phys. Rev. 98, 368 (1955).

[41]Because of our neglect of a possible "inhomogeniety temperature" in determining m^*, the value reported in Table II should be taken as an upper bound for the light holes. This source of error does not affect the heavy-hole m^* values (exponential rather than sinh amplitudes).

[42]B. L. Booth and A. W. Ewald, Phys. Rev. 168, 805 (1968).

[43]The magnetoconductivity data (Sec. III) imply that the heavy mass band is holelike. The deduction from LQO observations that this energy surface is warped out at [111] and in at [100] gives $|\alpha| > \beta$ in Eq. (10). But this inequality leads to the conclusion that the light carriers [minus sign in Eq. (10)] have the same sign as the heavy carriers, i.e., both are holes.

[44]J. A. Swanson, Phys. Rev. 99, 1799 (1955).

[45]Note that the electron mobility is about 15% less than the heavy-hole mobility (Table I). Assuming identical relaxation times, this would make the electron effective mass about 15% larger than the heavy-hole mass, or approximately $0.5m_0$, which with a g factor of 2, would lead to a nearly vanishing LQO amplitude (Ref. 32).